Solute transport in heterogeneous model porous media under different flow rates: Experimental and modelling study

Samer Majdalani, Vincent Guinot

This is the preprint of a paper published in Journal of Hydrology
(Volume 616, January 2023, 128790)

Solute transport in heterogeneous model porous media under different flow rates: experimental and modelling study

Samer Majdalani [a,*] and Vincent Guinot [a,b]

[a] HSM, Univ Montpellier, CNRS, IRD, Montpellier, France
[b] LEMON, Univ Montpellier, CNRS, HSM, Inria, IRD, Montpellier, France

* Corresponding author: Samer Majdalani
Email: samer.majdalani@umontpellier.fr

Highlights:
– High quality experimental data set for passive transport in heterogeneous porous media
– Flow rate independent and continuity preserving formulation for MRAD parameters confirmed by experiments
– Linearity of exchange and dispersion and exchange coefficients with respect to flow rate confirmed by the experimental data set

Keywords: flow rate, solute transport, heterogeneous model porous media, advection-dispersion, multi-region.

Abstract

The present paper focuses on solute transport behaviour in a Model Heterogeneous Porous Medium (MHPM) under different flow rates. We report tracer experiments under stationary hydraulic conditions, with 7 different stationary flow rates spanning two orders of magnitude. Several replicates are carried out on several MHPMs, allowing for a sound statistical assessment of experimental imprecision. The experimental BreakThrough Curves (BTCs) exhibit a dual transport mode in agreement with previously-reported field scale experiments. This dual transport mode is shown to be flow-rate independent under a suitable variable change, with the BTCs superposing in the limit of experimental uncertainty. The experiment is modelled using a classical Multi-Region Advection-Dispersion (MRAD) model with only two mobile regions. We present a flow rate independent reformulation of the MRAD model that that allows both water and solute continuity to be preserved during the calibration process. Assuming a linear dependence of the dispersion and exchange coefficients on the flow rate is shown to yield satisfactory model behaviour. This confirms the linearity of the dispersion coefficient with respect to the flow rate, often suggested in the literature, over a wide range of flow conditions.

1. Introduction

Laboratory experiments on model heterogeneous porous media MHPMs contribute to understand the behaviour of solute transport in real world situations (Majdalani et al., 2015). A large number of laboratory scale experimental studies on solute transport in porous media involve a single flow rate, while in real world situations the flow rate may vary over one or two orders of magnitude.

Several laboratory studies of solute transport in porous media have tested a variable flow rate in order to test its effect on modelling parameters. A wide review can be found in Griffioen et al. (1998), Maraqa (2001), and Haggerty et al. (2004). In these studies, the most widely used model is the Mobile-Immobile Model (MIM), based on the advection-dispersion equation where two regions (mobile and immobile) exchange mass between each other. The review of Griffioen et al. (1998) is based on 20 experiments. It shows correlations between the flow rate and the mass transfer coefficient, the mass transfer and the advection time scale, the mass transfer and diffusion time scales, the mass transfer and longitudinal interaction time scales. The review by Maraqa (2001) is based on 19 experiments. It shows that correlations exist between the mass transfer coefficient and the flow rate, or the mass transfer coefficient and the residence time. The review of Haggerty et al. (2004) is based on 316 experiments. Correlations are inferred between the effective mass transfer time and other parameters such as the flow rate, the capacity coefficient, the advective residence time and the experimental duration.

Experiments reported in the literature involve porous media made of sand (Coats and Smith, 1964; Gaudet et al., 1977; De Smedt et al., 1986; Rambow and Lennartz, 1993, Kookana et al., 1993 ; Sharma et al., 2022 ; Sutton et al., 2022), loam (van Genuchten and Wierenga, 1977; van Genuchten et al., 1977), loamy sand (Khan and Jury, 1990), clay (Jørgensen et al., 2004), stony soil (Schulin et al., 1987), glass beads (Krupp and Elrick, 1968; De Smedt and Wierenga, 1984; Berkowitz et al., 2009), field soil (Smettem, 1984, Sutton et al., 2022), loam and field soil (Selim et al., 1987), aggregate (Rao et al. 1980; Seyfried and Rao, 1987; Koch and Flühler, 1993; Li et al., 1994; Nkedi-Kizza et al. 1984; Brusseau et al., 1994; Bajracharya and Barry, 1997), or spherical clayey inclusions in sandy media (Tran Ngoc et al., 2020).

In the aforementioned studies, porous media are either homogeneous or moderately heterogeneous. Heterogeneity is generally obtained by introducing coarse aggregates into a finer surrounding medium (e.g. glass or clay beads into sand). Li et al. (1994) introduced random porous polyethylene cylinders (porosity 0.50) into silt soil (porosity 0.43). Bajracharya and Barry (1997) used a porous medium consisting of fine sand and polyethylene cylinders in different proportions for 3 experimental columns of different lengths, with a respective total porosity of the composite medium of 0.34, 0.36, and 0.40. Berkowitz et al. (2009) used a porous medium made of adjacent porous materials of fine (1 mm) and coarse (4 mm) glass beads, where the porosity (0.39) is the same in both fine and coarse media. Therefore, in literature studies, the porosity of the introduced heterogeneity mostly belongs to the range [0.5, 0.6], which is rather close to the porosity of the surrounding medium (range [0.3, 0.4]).

In many laboratory studies the flow rate varies over a single order of magnitude (Griffioen et al., 1998; Maraqa, 2001; Haggerty et al., 2004). Although reviews (Griffioen et al., 1998) report flow rate variations over several orders of magnitude, they aggregate several studies made on different media, that were all performed over one (or slightly more) order of magnitude. Rare are the studies where the flow rate in laboratory heterogeneous porous media is varied over two orders of magnitude within the same medium. One of the widest flow rate ranges is reported in Li et al. (1994), where the pore velocity is varied by a factor 54 and only

3 different flow rates are used. In the study by Bajracharya and Barry (1997), the pore velocity is varied by a factor 12.5.

As mentioned above, the laboratory porous medium of Li et al. (1994) and Bajracharya and Barry (1997) is moderately heterogeneous. Moreover, the flow direction in these studies is vertical upward (from bottom to top of the column). We argue that salt-based solute transport experiments under upward flow are liable to induce density effects and that the observed BreakThrough Curves (BTCs) might not reflect the real behaviour of passive transport. In fact, rare are the studies of solute transport in porous media using salt tracer that take the possibility of solute density effects into account and their impact on BTCs. Due to gravity, strongly concentrated solute may be trapped in lower parts of the porous medium, thus impacting the behaviour of solute transport and biasing the breakthrough curves compared to those of purely passive transport.

Another issue concerning experimental data is reliability. In the aforementioned studies, rare are the solute transport experiments where both the experiment and the porous medium are replicated. The first point means that one should repeat the same experiment several times on a given porous medium column, while the second point means that one should construct several identical porous medium columns and that the ensemble of the experimental protocol should be repeated on each of them. By taking the mean of all replicates, as well as the minimum and maximum values, the statistical variability of the breakthrough curves stemming from various sources can be assessed. Not only is statistical variability of great help in estimating modelling parameters, but it also gives stable and reliable breakthrough curves by minimizing realization sampling effects.

In this paper, we study solute transport in laboratory scale Model Heterogeneous Porous Media (MHPMs) under different flow rates. The flow rate Q of tracer step experiments varies over two orders of magnitudes: the ratio of the maximum to the minimum flow rate is 100. The flow rate is modified across the different realizations/experiments but not within a single realization (the flow in each given experiment is stationary). The Model Heterogeneous Pours Medium (MHPM) used in the present study is strongly heterogeneous. A rectangular cavity (porosity 100%) is introduced into surrounding glass beads (porosity 40%). The purpose is to assess the applicability of standard transport models to strongly heterogeneous media, in order to determine whether the degree of heterogeneity induces limitations in the model. Besides, solute transport experiments are done with horizontal flow and we make sure that no solute density effect is present in the MHMP. All tracer step experiments are replicated (see Section 2): each experiment is replicated 3 times and the ensemble of the experimental protocol is replicated on 3 different MHPMs built under the same specifications.

We simulated the breakthrough curves by a classical approach based on the multi-region advection-dispersion (MRAD) model as presented and analyzed in Majdalani et al. (2018), where only two mobile regions are used. The MRAD model is a generalization of well-known models such as the Two Region (TR), Mobile-Immobile (MI) and Multi-rate models (Coats and Smith, 1964; Griffioen et al. 1998; Haggerty et al., 2000; van Genuchten and Wierenga, 1976). A number of studies have focused on how the model parameters behave with the flow rates (Griffioen et al., 1998; Haggerty et al., 2004; Li et al., 1994). They do not all lead to the same conclusions and a wide variety of behaviours is reported. Little is known about how the parameters were constrained in the model calibration process. In particular, it is not always clear whether water and solute mass conservation were enforced in the calibration process. In other words, it is not always clear whether the flow rate in the model is identical to that prescribed in the experiments. Not preserving this condition may yield biases in the calibrated transport parameters. In the present work, mass conservation is enforced by rewriting the MRAD model in terms of flow rate-independent parameters, among which a discharge partition coefficient for the various regions in the model. To our best knowledge, such a

reformulation has not been presented in the literature before. Obviously, many other modelling formalisms than the MRAD might be used. More complex models such as Multi-rate models (Haggerty and Gorelick, 1995) and fractional dynamics / Continuous-Time Random Walk (CTRW) models have proven efficient in the modelling of tailing effects and transient dispersion (Berkowitz et al., 2008 ; Bijeljic, 2006 ; Le Borgne et al., 2011 ; Sun et al., 2014 ; Moradi and Mehdinejadiani, 2018). Multi-region versions of these approaches have been presented recently (Sun et al., 2020; Yin et al., 2021). Such models are particularly efficient in modelling the long-term behaviours and tailing effects in breakthrough curves that are typical of anomalous transport. They can account for asymptotically long travel times resulting from trapping as well as sudden jumps over long distances, known as Levy flights (Klafter et al., 1987 ; Metzler and Klafter, 2000). However, in the present study, heavy tailing was not identified as a salient characteristic of the BTCs. For this reason, using this type of model was not deemed necessary.

The present paper is organized as follows. Section 2 presents the materials and methods. Subsections 2.1 and 2.2 are devoted respectively to the experimental setup and protocol for obtaining a wide range of transport conditions in a strongly porous heterogeneous medium, with flow rates spanning two orders of magnitude. Subsection 2.3 presents a continuity-enforcing writing of the MRAD model. Subsection 2.4 deals with the calibration approach, that takes experimental imprecision into account. Section 3 presents the experimental and modelling results. Sections 4 and 5 are devoted respectively to a discussion and conclusion.

2. Material and Methods

2.1. Model heterogeneous porous medium X_i (i = 1 to 3) and Y_i (i = 1 and 2)

Three parallelepiped (Length 20 cm, height 2 cm, width 10 cm) columns (X_1, X_2, and X_3) were built manually by pasting 5 mm thick plastic plates. The X_i columns are labelled MHPM A, MHPM B, and MHPM C hereafter. They all contain a parallelepiped pore (length 15 cm, height 2 cm, width 1 cm) on one side. The rest of the column is filled with 1 mm glass beads (Figure 1). The rectangular pore (100% porosity) plays the role of a heterogeneity where water rapidly flows in comparison to the surrounding 1 mm glass beads (40% porosity). The ends of the rectangular pore are covered with 500 µm sieve so that the 1 mm glass beads cannot penetrate into it. The X_i columns have four inlets and four outlets. One inlet/outlet faces the rectangular pore, the remaining three inlets/outlets are spread over the width of the MHPM. The pore volume of each MHPM is V_0 = 158.8 ml.

To reduce solute density effect, the height of the MHPMs was taken very small (2 cm) in comparison to the width (10 cm) and length (20 cm). The assumption of negligible density effects was verified as follows. Two rectangular columns Y_1 (Figure 2) and Y_2 (Figure 3) were designed in a manner that if they are turned upside down, the position of the heterogeneity would change along the middle horizontal plane. Thus, should solute density effects be present, solute transport differ for the Up and Down positions in both Y_1 and Y_2 columns, and the resulting BTCs would be different.

2.2. Tracer step experiment: setup and protocol

The solute transport is studied using tracer step experiments under saturated conditions. The columns are first filled with deionized water, then a step of salty water (NaCl) with a concentration of C_0 = 0.05 M is introduced into the column via a peristaltic pump (Lead Fluid^{TM}). This yields an Atwood number $A = 2.9\times10^{-3}$, suggesting that density effects will be negligible. The concentration at the column output is given by a conductivity meter (WTW TetraCon 325^{TM}). The flow rate is estimated by weighing the effluents on a scale (Figure 4). The conductivity meter and the scale are connected to a data logger that samples the measurements at regular time intervals. The step experiment is stopped when the concentration at the column output reaches C_0 (concentration at the column input). The flow is maintained with pure, deionized water until the conductivity of the outflowing concentration returns to its initial, background level.

Each of the three X_i columns underwent step experiments with seven flow rates varying from 0.25 to 25 l/h (Table 1). The flow rate is varied across different realizations/experiments but not within a single experiment (the flow is constant during a given step experiment). Since the tested flow rates vary in ratios of 2, 4, 10, 20, 40, 100 and 200, they are lalelled Q_2, Q_4, Q_{10}, Q_{20}, Q_{40}, Q_{100}, and Q_{200} hereafter. For the lowest flow rate (Q_2), the duration of the step experiment was 3 hours and the data sampling interval wass 10 seconds. For the higher flow rate (Q_{200}), the duration of the step experiment was 2 minutes and the data sampling interval was 1 second (Table 1). Each step experiment was replicated three times for each of the three X_i columns, hence a total 7 × 3 × 3 = 63 experimental BTCs (see Results and Discussion sections).

The Y_1 and Y_2 columns underwent step experiments with the seven flow rates indicated in Table 1 but the duration of the Y_i experiments are smaller than those of X_i because the volume of Y_i columns is smaller than that of X_i columns. A selection of the BTCs for the Y_i columns is coemmented in the Results and Discussion sections.

2.3. MRAD Model

2.3.1 Model presentation

The so-called Multi-Region Advection-Dispersion (MRAD) (Majdalani et al. 2018) model is a generalization of a variety of models introduced in the literature from the 1970s. Two well-known particular configurations are (i) the Two Region (TR) model (Coats and Smith, 1964; Griffioen et al. 1998) and its particular implementation known as the Mobile-Immobile (MI) model (van Genuchten and Wierenga, 1976), and (ii) the MultiRate (MR) model (Haggerty et al., 2000). The general model consists of R regions, each of which may be mobile or immobile with its own flow and dispersion characteristics, exchanging mass with each other. The governing equations can be written in vector form as

$$\frac{\partial \mathbf{c}}{\partial t} + \frac{\partial}{\partial x}\left(\mathbf{U}\mathbf{c} - \mathbf{D}\frac{\partial \mathbf{c}}{\partial x}\right) = \mathbf{K}\mathbf{c} \quad (1a)$$

$$\mathbf{c} = [c_i], \quad \mathbf{U} = \mathrm{diag}(u_i) \quad (1b)$$

$$\mathbf{D} = \mathbf{U}\boldsymbol{\alpha}, \quad \boldsymbol{\alpha} = \mathrm{diag}(\alpha_i) \quad (1c)$$

$$\mathbf{K} = \boldsymbol{\mu}^{-1}[k_{ij}]\ ,\ \ k_{ij} = -\,k_{ji}\ \forall\ (i,j)\ ,\ \ \sum_j k_{ij} = 0\ \ \forall i \tag{1d}$$

$$\boldsymbol{\mu} = \mathrm{diag}(\mu_i) \tag{1e}$$

Where c_i, D_i, u_i, α_i, and μ_i are respectively the concentration, dispersion coefficient, flow velocity, dispersivity and volume fraction for Region i (i = 1,…, R), and k_{ij} is a first-order exchange coefficient between Regions i and j. The antisymmetry property for the matrix **K** and the zero sum in Equation (1d) are necessary conditions for mass conservation (Majdalani et al. 2018).

Specifying appropriate (μ_i, k_{ij}) combinations allow arbitrary exchange functions between the mobile and immobile regions to be modelled, including transfer functions with multiple transfer time scales and long-term memory effects (Haggerty et al. 2000, 2004). The model is also able to represent the transition from ballistic behaviour (i.e. variance of solute position growing proportionally to the square of travel time) at small spatial and time scales to normal (i.e. Fickian) dispersion at large scales (Majdalani et al. 2018). Moreover, Fickian behaviours can be obtained without including any dispersion terms by specifying appropriate velocities and exchange coefficients between parallel regions (Majdalani et al. 2018). In the most general possible layout (Figure 5), each region may exchange with all the other regions. Intuition suggests that exchange should be possible only between two regions that have similar flow velocities. This would ensure a smooth transition between low velocity (or immobile regions) and fast flowing regions. However, in a strongly heterogeneous porous medium, fast flowing regions may be located in the immediate neighbourhood of slow flow regions (Figure 5a), and the regions may not necessarily be connected. Therefore, as far as flow topology is concerned, nothing should preclude an exchange between any two different flow regions in the general case. The exchange coefficient in the model of Figure 5b reflects not only the transfer rate between the various regions, but also their degree of connectivity.

2.3.2 Identifying a flow rate-independent formulation for the MRAD model from experimental breakthrough curves

The question arises of how the model parameters, i.e. the coefficients of the matrices **U**, **D** and **K** vary with the flow rate Q. The simplest possible assumption is that **D**, **K** and **U** are proportional to the discharge and that $\boldsymbol{\mu}$ is fixed. These assumptions can be checked easily from the experimental breakthrough curves. To do so, the following variable change $\omega = Qt/V_0$ is introduced, where V_0 is the flow volume in the domain. This volume can be determined from the experimental breakthrough curves $c_B(t)$ by noting that the inflow concentration signal c_{in} is a step function with amplitude c_0:

$$Q\int_0^T (c_0 - c_B(t))dt = V_0 c_0 \tag{2}$$

which yields

$$V_0 = Q\int_0^T \left(1 - \frac{c_B(t)}{c_0}\right)dt \tag{3}$$

The integral is computed from the experimental values using the trapezium rule for numerical integration. Performing the variable change $\omega = Qt/V_0$ in Equation (1a), using (1b)-(1e) leads to

$$\frac{\partial \mathbf{c}}{\partial \omega} + \frac{\partial}{\partial x}\left(\frac{V_0}{Q}\mathbf{U}\mathbf{c} - \frac{V_0}{Q}\mathbf{U}\boldsymbol{\alpha}\frac{\partial \mathbf{c}}{\partial x}\right) = \frac{V_0}{Q}\mathbf{K}\mathbf{c} \tag{4}$$

In the particular case where **K** and **U** are proportional to Q and the dispersivities α_i are independent of Q, all the matrix coefficients in equation (4) are Q-independent and all plots of $\mathbf{c}(x, \omega)$ obtained for different values of Q superimpose. From an experimental point of view, only the BTC is known:

$$c_{\mathrm{B}}(\omega) = \frac{\sum_i \mu_i u_i c_i(x_{\mathrm{ds}}, \omega)}{\sum_i \mu_i u_i} \tag{5}$$

where x_{ds} is the abscissa of the downstream end of the model. Therefore, for the BTCs $c_{\mathrm{B}}(\omega)$ to superimpose, the volume fraction matrix $\boldsymbol{\mu}$ must be independent of Q.

2.3.3 New MRAD formulation

The MRAD model studied here is not different conceptually from those presented earlier in the literature. The only difference lies in the presentation of the equations and in the identification of the model parameters. The proposed formulation brings the following improvements over previously published versions:

– the (assumed) proportionality of the dispersion and exchange coefficients to the flow rate is incorporated directly in the formulation,
– the new formulation intrinsically enforces conservation of both water and solute regardless of the flow rate. Such conservation is not enforced in usual calibration approaches (such as that described in Majdalani et al. (2018)), whereby the flow velocities and volume fractions are calibrated without constraining the conservation of water flux (let alone solute fluxes).

The flow is divided into R regions flowing in parallel. Let A_i and Q_i be respectively the cross-sectional area and discharge in Region i. They are related to the total area A and discharge Q with

$$A_i = \mu_i A, \quad Q_i = A\mu_i u_i = \nu_i Q \tag{6}$$

Assuming discharge-proportional dispersion and exchange coefficients, the governing equation in Region i is

$$A_i \frac{\partial c_i}{\partial t} + \frac{\partial}{\partial x}\left(Q_i c_i - \frac{\partial}{\partial x}(Q_i \alpha_i c_i)\right) = Q \sum_{j \neq i} k_{ij}(c_j - c_i) \tag{7}$$

Substituting the relationships (6) into (7) yields

$$\mu_i A \frac{\partial c_i}{\partial t} + \frac{\partial}{\partial x}\left(\nu_i Q c_i - \frac{\partial}{\partial x}(\nu_i Q \alpha_i c_i)\right) = Q \sum_{j \neq i} k_{ij}(c_j - c_i) \tag{8}$$

The vector form of the equation is

$$A\boldsymbol{\mu} \frac{\partial \mathbf{c}}{\partial t} + \frac{\partial}{\partial x}\left(Q\boldsymbol{\nu}\mathbf{c} - \frac{\partial}{\partial x}(Q\boldsymbol{\nu}\boldsymbol{\alpha}\mathbf{c})\right) = Q\mathbf{K}\mathbf{c} \tag{9a}$$

$$\boldsymbol{\mu} = \mathrm{diag}(\mu_i), \quad \boldsymbol{\nu} = \mathrm{diag}(\nu_i) \tag{9b}$$

$$K_{ij} = -K_{ji} = k_{ij} \quad \forall\, i \neq j \tag{9c}$$

$$K_{ii} = -\sum_{j \neq i} K_{ij} \tag{9d}$$

where K_{ij} and k_{ij} stand respectively for the elements of the matrix **K** and the exchange coefficients between the regions. Equation (9a) is rewritten as

$$\frac{\partial \mathbf{c}}{\partial t} + \frac{\partial}{\partial x}\left(\frac{Q}{A}\boldsymbol{\Theta}\mathbf{c} - \frac{\partial}{\partial x}\left(\frac{Q}{A}\boldsymbol{\Theta}\boldsymbol{\alpha}\mathbf{c}\right)\right) = \frac{Q}{A}\boldsymbol{\mu}^{-1}\mathbf{K}\mathbf{c} \tag{10a}$$

$$\boldsymbol{\Theta} = \boldsymbol{\mu}^{-1}\boldsymbol{\nu} = \mathrm{diag}\left(\frac{\mu_i}{\nu_i}\right) \tag{10b}$$

Noting that $A = V_0/L$, (L is the length of the column) one has

$$\frac{\partial \mathbf{c}}{\partial t} + \frac{\partial}{\partial x}\left(\frac{QL}{V_0}\boldsymbol{\Theta}\left(\mathbf{c} - \frac{\partial}{\partial x}(\boldsymbol{\alpha}\mathbf{c})\right)\right) = \frac{QL}{V_0}\boldsymbol{\mu}^{-1}\mathbf{K}\mathbf{c} \tag{11}$$

For a two region model as dealt with in the present work, there are 5 independent parameters: α_1, α_2, μ_1, ν_1, and k_{12}. Note that $\mu_2 = 1 - \mu_1$ and $\nu_2 = 1 - \nu_1$. In the absence of dispersion and exchange ($a_1 = a_2 = k_{12} = 0$), the analytical solution for a step injection consists of two steps arriving at the downstream end of the MHPM at two different times (dashed line in Figure 6, top). Increasing the dispersion coefficients α_1 and α_2 tends to smooth out these steps (solid line in Figure 6, top). (μ_1; μ_2) act on the contrast between the arrival times of the two steps, while ν_1 influences their relative sizes. Increasing k_{12} tends to smooth out the transition between the two steps (Figure 6, bottom). Note that the above considerations are only indicative of the broad influence of the various parameters on the modelled solution. They do not reflect the interactions between the exchange and dispersion parameters that may have similar effects on the long term behaviour of the solution. For instance, the theoretical analysis in Majdalani et al. (2018) shows that a Fickian dispersive behaviour is obtained asymptotically for $\alpha_1 = \alpha_2 = 0$, provided that the exchange coefficient k_{12} is non-zero.

Note that the coefficients in matrix **K** have the dimension of the inverse of a length. Owing to the conservation properties (9c), (9d), **K** has at least one nil eigenvalue, while the remaining ones are all negative (Majdalani et al., 2018). The smaller of the absolute values of the remaining eigenvalues gives an order of magnitude of the distance needed for the concentrations in all regions to homogenize. Beyond this distance, the standard, single region, Fickian dispersion model becomes valid, even if the dispersion coefficients are zero in all regions (Majdalani et al., 2018). In the case of a two region model as explored in the present study, the non-zero eigenvalue is equal to $-2k_{12}$, which yields a characteristic distance $(2k_{12})^{-1}$. Note that this holds in the case of zero dispersion coefficients α_i in all regions. In the presence of dispersion, front spreading occurs faster in all regions and the normal, Fickian dispersion regime is achieved over smaller distances.

2.4 Calibration

The model parameters are calibrated as introduced in Majdalani et al. (2018) by minimizing the objective function

$$J = \sum_k e_k^{(1)} e_k^{(2)} \tag{12a}$$

$$e_k^{(1)} = \left(\frac{1}{T - t_0}\int_{t_0}^{T} \max\left(0, \left|c_B - c_{exp}\right| - \delta c\right)^2 (t)\mathrm{d}t\right)^{1/2} \tag{12b}$$

$$e_k^{(2)} = \left(\frac{1}{1/T - 1/t_0}\int_{t_0}^{T} \max\left(0, \left|c_B - c_{exp}\right| - \delta c\right)^2 (t)\mathrm{d}\left(\frac{1}{t}\right)\right)^{1/2} \tag{12c}$$

where c_B and c_{exp} are respectively the simulated and experimental breakthrough concentrations, $t_0 > 0$ and T are respectively the simulation time step and simulation length,

and δc is the measurement precision. The max() operator ensures that the modelling error is zero if the difference between the simulated and experimental concentrations is smaller than the measurement precision δc.

The square root of J thus provides a measure of the difference between the modelling results and the experiments. It is to be compared with the experimental imprecision, that is measured by computing the standard deviation of the various replicas of a given experiment:

$$\sigma_{\text{av}} = \frac{1}{N}\sum_{i=1}^{N}\frac{1}{T_i}\int_0^{T_i}\sigma_i(t)\,\mathrm{d}t \tag{13a}$$

$$\sigma_i(t) = \left(\frac{1}{m-1}\sum_{j=1}^{m}\left(c_{\text{exp},i,j}(t) - \overline{c_{\text{exp},i}}(t)\right)^2\right)^{1/2} \tag{13b}$$

$$\overline{c_{\text{exp},i}}(t) = \frac{1}{m_i}\sum_{j=1}^{m_i} c_{\text{exp},i,j}(t) \tag{13c}$$

where $c_{\text{exp},i,j}(t)$ is the experimental concentration measured at time t for the jth replica of the ith flow rate, m_i is the number of replicas done for the ith flow rate, $N = 6$ or 7 is the number of flow rates tested, and T_i is the length of the experiment for the ith flow rate. $\overline{c_{\text{exp},i}}(t)$ is therefore the average at time t of all the concentrations obtained from the m_i replicas done for the ith flow rate, and $\sigma_i(t)$ is a measure of the experimental dispersion, at a given time t, of the various replicas for the ith flow rate. Averaging σ_i over time and over the N flow rates yields σ_{av}, a measure of the overall dispersion of the experimental concentration time series about the mean signal for all times and all flow rates.

3. Results

3.1. Solute density effect (Y_i columns)

Columns Y_1 and Y_2 are only test columns to verify the existence or the absence of solute density effect. Since the position of the heterogeneity is not the same in Y_i columns whether they are in Up or Down position (Figures 2 and 3), and since the solute has a tendency to dive to the bottom due to gravity (water + solute is denser than deionized water), gravity effects would induce differences between the BTCs of Columns Y_1 and Y_2 would be different in Up and Down positions. We made step experiments on Columns Y_1 and Y_2 in Up and Down positions with all the flow rates given in Table 1 and we noticed that the BTCs were the same (in the limit of experimental uncertainty) in Up and Down positions, regardless of the flow rate. As an illustration, Figure 7 (top) (respectively bottom) shows the breakthrough curves of column Y_1 (respectively Y_2) in Up and Down positions for Flow rate Q_{100}. Therefore, as argued in Section 2, solute density effects are negligible with the present MHPM design.

3.2. Flow rate effect (X_i column or MHPM A, B, and C)

Each of the three X_i columns underwent step injections under the seven flow rates Q_2 – Q_{200}, with three replicates in each case. As suggested previously in the MRAD formulation, we adopt the variable change $\omega = Qt/V_0$ to plot the BTCs. Figure 8 shows that, for every MHPM (A, B, and C), the resulting experimental breakthrough curves superimpose in the limit of

experimental imprecision for all flow rates. This validates the assumption of a model formulation with discharge-independent parameters, as expressed by Eq. (4).

In homogeneous porous media, BTCs classically exhibit an 'S' shape. The BTCs shown in Fig. 8 have a double 'S' shape: the lower 'S' is attributed to a fast solute transport mode through the heterogeneity (rectangular pore), while the higher 'S' is attributed to a slower transport mode within the glass beads. Other studies have also noticed that BTCs in heterogeneous porous media do not have a classical 'S' shape (Silliman and Simpson, 1987 ; Golfier et al., 2011 ; Majdalani et al., 2015). Double 'S' shaped BTCs (or double peak curves for their derivatives) have also been reported in natural/real media (Maloszewski et al., 1992 ; Goldscheider et al., 2008 ; Perrin and Luetscher, 2008 ; Field and Leij, 2012 ; Dewaide et al., 2018).

3.3. MRAD simulations results

The calibration results are given in Table 2. Noting that the error J is the product of two Root Mean Square Errors (RMSEs), one with respect to t and the other with respect to $1/t$, $J^{1/2}$ gives a meaningful assessment of the difference between the simulated and experimental breakthrough curves. $J^{1/2}$ is about 3% of the total variation in the concentration, which can be deemed a very good agreement between the model and the experiment. In comparison, the experimental imprecision ranges from 0.56% to 1.56% (i.e. half of the modelling error). Figure 9 shows the experimental versus simulated breakthrough concentrations. A satisfactory alignment over the first bisector is observed. This was expected considering the values of $J^{1/2}$ in Table 2.

Since the behaviour of the breakthrough curve for the Q_{200} setting in Figure 8 seems different from that of the other BTCs, a second calibration of the model is run by removing the Q_{200} time series from the experimental data set. This leads to slightly better calibration results (Table 3), with $J^{1/2}$ reduced by 10% to 25% compared to the calibration results in Table 2. Removing Q_{200} from the experimental data set leaves the average experimental imprecision almost unchanged. Comparing the average calibrated parameter values in Tables 2 and 3 shows that the calibrated α_1, μ_1 and k_{12} are significantly sensitive to the presence of Q_{200} in the data, while a_2 and v exhibit a much lower sensitivity.

Table 4 shows the r^2 coefficients, the objective function $J^{1/2}$ and the Mean Bias Error (MBE), computed from the experimental vs. simulated C/C_0 series shown in Figure 9. The MBE is calculated accounting for experimental imprecision as

$$\mathrm{MBE} = \frac{1}{T-t_0}\int_{t_0}^{T}\left[\max\left(0, c_B - (c_{exp} + \delta c)\right) + \min\left(0, c_B - (c_{exp} - \delta c)\right)\right](t)\,dt \qquad (14)$$

whereby the modelling error is calculated as the difference between the modelled concentration signal c_B and the closest bound of the experimental concentration interval $[c_{expe} - \delta c, c_{expe} + \delta c]$.

All r^2 coefficients are larger than 0.99, even for the Q_{200} setting. The values for $J^{1/2}$ (that is analogous to a Root Mean Squared Error) is smaller than 1.6×10^{-2} in all 21 experiments, and about 5×10^{-3} for most of them. Lastly, the MBE is smaller than 1%. For all three indicators, the Q_{200} setting does not significantly poorer values than for the other flow rates. For instance, for MHPM A, the r^2 for Q_{200} is similar to that of Q_{10}, its MBE is smaller and its $J^{1/2}$ is very similar. Similar remarks can be made for MHPM B and MHPM C. This confirms that the behaviour of the model is satisfactory, not only on the average, but also for all individual experiments for all three MHPM.

4. Discussion

The linearity of the exchange coefficient k_{12} and the dispersion coefficients D_i with respect to the flow rate under laminar flow was expected from theoretical considerations (Majdalani et al., 2018), because these coefficients reflect the statistics of the fluctuations of the velocity field about the mean values. Such fluctuations are expected to be proportional to the average flow velocity (thus to the flow rate) when the flow rate is small.

The present experimental and modelling results confirm the theoretical assumption of a linear relation between the flow rate and the mass exchange coefficients over a wide range of flow rate values, even for a strongly heterogeneous MHPM. This is also true for the flow velocities and dispersion coefficients in the two regions of the model. The volume fractions of the two regions and the partition coefficient of the flow rate between these regions are found to be flow rate independent. As a consequence, the flow velocity is proportional to the flow rate and the dispersivity is flow rate independent in both regions. We note that e.g. Hansen (2022) also inferred a flow velocity proportional to the flow rate and a flow rate independent dispersivity using a very different experimental setup and a different model, based on fractional mass exchange between the mobile and immobile regions. While Hansen (2022) concludes that the exchange coefficient is flow rate independent, we obtain a linear relationship between k_{12} and the flow rate. These two findings are not necessarily contradictory in that the structures of the two exchange models are different.

The three MHPMs used in the present study were built following the same geometric specifications. They are identical within a geometric precision of 1 mm (for a total length of 150 mm). This may be considered an excellent geometric replicability. Comparing the calibration results in Tables 2 and 3 gives an idea of the uncertainty in the parameters with respect to MHPM manufacturing for almost indiscernible geometries. While the volume and flow distribution parameters μ_i and v_i in Table 2 are remarkably stable from one MHPM to the next, the dispersion coefficients in both regions vary by 150% and the exchange coefficient varies by more than 300%. Dropping the largest discharge from the experimental set contributes to increase the consistency of the calibration results: all model parameters, including the exchange coefficient k_{12}, are remarkably consistent for all MHPMs. This seems to indicate that the highest flow rate (Q_{200} pump setting) is the limit of applicability of the flow rate independent model formulation. For this flow rate, the residence time of the tracer within the MHPM is approximately 23 s, which corresponds to an average flow velocity of 6.6 mm/s. Assuming that all the flow passes through the 2 cm high central conduit yields an upper bound Re = 132 for the Reynolds number. Turbulence effects are therefore an unlikely cause. However, it is suspected that, owing to the strongly contrasted MHPM geometry, the effective flow paths are not exactly the same for the Q_{200} setting as for smaller flow rates, thus inducing different model calibration results.

In order to compare our modelling results with previous literature findings, namely Li et al. (1994) and Bajracharya and Barry (1997), we recall that in the present study u varies between 0.2 and 20 cm/min. Li et al. (1994) found a linear relation between u and the mass exchange coefficient k_{12} for $0.3 < u < 2.7$ cm/min, but for $0.05 < u < 0.1$ cm/min the relation between k_{12} and u was rather quadratic ($k_{12} = 94.23 \times u^{2.3}$). In both cases, the fit of the k_{12}–u relationship was based on 3 data points, for which the experimental confidence interval is not known. Thus, according to Li et al. (1994), the k_{12}–u relationship is quadratic at low pore water velocity and linear at higher velocities. We argue that more than 3 data points are needed to deduce a good fit and this is why we use 7 flow rates in our study. In our study, the k_{12}–u relationship is linear, in agreement with Li et al. (1994) for high velocities, and even beyond the range of velocities explored by Li et al. (1994).

Bajracharya and Barry (1997) tried to fit a relation in the form $k_{12} = au^b$ to their data and evaluated the fitting quality using the coefficient of determination r^2. Since several, different experimental conditions (column material, column depth, column diameter, velocity range) were involved, Bajracharya and Barry (1997) obtained several values for the power b: b = 2.15 (r^2 = 0.965) for 0.05 < u < 0.4 cm/min, b = 1.79 (r^2 = 0.971) for 0 < u < 0.8 cm/min, b = 1.3 for 0 < u < 6 cm/min (r^2 = 0.954). In the latter case, a linear relation with b = 1 was also possible with r^2 = 0.933. Bajracharya and Barry (1997) concluded that k_{12}–u relationship follows a power law with a power coefficient b that ranges from 1 to 2 where k_{12} scales linearly with u at low pore water velocity, and k_{12} may assume any value between 0.5 and 2 at higher velocities (which contradicts the conclusions of Li et al. (1994)).

In the review of Maraqa et al. (2001), that is based on 19 experiments, the k_{12}–u relationship is found to be sublinear (b < 1) and the value of b depends on the type of porous medium: b = 0.85 (r^2 = 0.57) for a non-aggregated medium with 0.01 < u < 0.12 cm/min, b = 0.71 (r^2 = 0.52) for an aggregated medium with 0.01 < u < 0.12 cm/min, and b = 0.76 (r^2 = 0.7) for a stony medium with 0.006 < u < 0.045 cm/min.

The review of Griffioen et al. (1998) is based on 20 experiments. Its conclusions are that the k_{12}–u relationship rather follows $k_{12} = au^b$, where b has no stable value. Table 3 in Griffioen et al. (1998) shows that b can take any value between -0.3568 (experiment of Khan and Jury (1990)) and 4.8543 (experiment of Nielsen and Biggar (1961)).

The results of Bajracharya and Barry (1997), Maraqa et al. (2001), and Griffioen et al. (1998) show that, even though the relationship k_{12}–u is expected to be linear for theoretical reasons, experimental data do not generally reflect such linearity. However, such lack of linearity may stem from various sources. For instance, solute density effects may be present under vertical flow conditions and induce a non-linear behaviour in the k_{12}–u relationship. The lack of linearity may also be explained by the absence of replicates. Not replicating the measurements precludes the width of the experimental confidence interval to be assessed, thus making it impossible to determine whether a linear (or another type of) law would pass through the experimental error boxes. We consider that our experimental data set is reliable because the absence of solute density effects has been verified experimentally and because tehere are 9 replicates for each flow rate: 3 replicates of each experiment and 3 replicates of the porous medium.

A last discussion point is how the conclusions of the present work, carried out using a single, strongly contrasted heterogeneity, can be transposed to more natural aquifers, involving much larger scales and less contrasted heterogeneities. The present MHPMs were designed so as to maximize the contrast between the fast and slow flow paths. The purpose was to make the experimental transport process as difficult as possible to model using the standard MRAD model. From the authors' experience on MHPMs placed in series (Majdalani et al., 2015), increasing the number of heterogeneities tends to smooth out the transport process, bringing it closer to a Fickian behaviour. This is nothing but a consequence of the central limit theorem (see e.g. Klafter et al., 1987 ; Metzler and Klafter, 2000). Decreasing the contrast between the permeabilities of the two media or making the volume occupied by one of them significantly smaller than the other also contributes to decrease the contrast between the slow and fast transport fluxes, which also brings the BTCs closer to those of a single transport mode, Fickian behaviour. That the reformulated MRAD model reproduces satisfactorily the BTCs of a single, highly contrasted MHPM is therefore seen as an encouraging sign for the modelling of more natural aquifers containing multiple heterogeneities. Obviously, this conclusion holds only provided that the properties (size, porosity, permeability) of the heterogeneities do not exhibit large scale variations that would be impossible to capture by a model with uniform parameters.

5. Conclusion

In this paper we studied solute transport in heterogeneous model porous medium under a wide range of flow rates. We conducted tracer experiments with seven tested flow rates ranging from 0.25 to 25 l/h, that is over two orders of magnitude. In comparison to other studies where the porous medium is moderately heterogeneous, our experiment is characterized by a high degree of heterogeneity. Solute transport experiment were carried out under horizontal flow and so that no solute density effects are present in the MHPM. In order to make our experimental data reliable for modelling exercise, all tracer step experiments were done with replicates: 3 replicates of each experiment and the ensemble of the experimental protocol was replicated on 3 identical MHPMs (A, B, and C).

The experimental breakthrough curves show a double 'S' shape behaviour in accordance with other literature findings, and that the 'S' shape is a stable behaviour that does not vary with flow rate under a suitable change of variable on the abscissa axis: $\omega = Qt/V_0$. This shows that there exists a model with flow-rate independent parameters that can reproduce all experimental BTCs. The BTCs are modelled successfully using a reformulated version of the MRAD model with only two mobile regions. The new formulation enforces mass balance for both water and the solute, and uses flow rate independent parameters. The simulated BTCs are in close agreement with the experimental ones, with an error around 3%, r^2 coefficients above 0.99 and a Mean Bias Error smaller than 10^{-2}. This validates the assumption of linear flow velocities, dispersion coefficients and exchange coefficients with respect to the flow rate in the two region model.

Although the assumption of linearity between transport parameters and the flow rate has been suggested in previous studies, no clear experimental evidence for this can be found in the literature. Our study can be considered to provide a clear experimental evidence of the linearity assumption between MRAD parameters and flow rate. The variability of the model parameters from one MHPM to the other is strongly reduced when the largest flow rates are dropped from the experimental data sets. This may be an indication that the largest flow rate is at the limit of model applicability. Our experimental data set is deemed reliable owing to its high sampling rate, the use of several replicates for each experiment, all done on several replicates of the MHPM.

We should like to conclude with a remark on the one-dimensional nature of the transport model. Although MHPMs (and the resulting flow within them) are three-dimensional, most experiments performed in the literature (including the present ones) involve one-dimensional flow models. These are upscaled models (Farmer, 2002) in that they attempt to provide a one-dimensional representation of the transport process on the (low) resolution of the MHPM size, while the actual transport process is spatially variable and three-dimensional on a much smaller scale. Being one-dimensional, the model includes a single (longitudinal) dispersion coefficient. However, in real-world situations, dispersion involves a tensor formulation with three principal directions. A logical next step in the present research should be to investigate of how the MRAD model can be generalized to two- and three-dimensional modelling and whether the rate of convergence to the Fickian limit and the linear dependence to the flow is preserved when the MHPM is not only strongly heterogeneous but also strongly anisotropic in two and three dimensions.

Appendix. Numerical solution of the transport equations

The present appendix details the numerical solution of the transport equation (1a), that can be rewritten in the following form under the assumption of space-independent coefficients in the equation

$$\frac{\partial \mathbf{c}}{\partial t} + u_i \frac{\partial c_i}{\partial x} - D_i \frac{\partial^2 c_i}{\partial x^2} = -\sum_{j \neq i} \mu_i k_{ij} c_j \tag{A.1}$$

The equation is solved using a three step time splitting procedure (Strang, 1968). To do so, Eq. (A.1) is split into three equations:

$$\frac{\partial \mathbf{c}}{\partial t} + u_i \frac{\partial c_i}{\partial x} = 0 \tag{A.2a}$$

$$\frac{\partial \mathbf{c}}{\partial t} - D_i \frac{\partial^2 c_i}{\partial x^2} = 0 \tag{A.2b}$$

$$\frac{\partial \mathbf{c}}{\partial t} = -\sum_{j \neq i} \mu_i k_{ij} c_j \tag{A.2c}$$

where Eqs. (A.2a-c) are solved numerically using the same computational time step Δt, and each equation (A.2b-c) uses the result of the previous one as a starting point over the time step.

Equation (A.2a) is solved using a finite volume procedure. Within each region i (the subscript i is dropped in the notation for the sake of readability), the following formula is used:

$$c_k^{n+1} = c_k^{n+1} + \frac{u\Delta t}{\Delta x}\left(c_{k-1/2}^{n+1/2} - c_{k+1/2}^{n+1/2}\right) \tag{A.3}$$

where c_k^n is the average value for c in the kth cell at time step n, and $c_{k-1/2}^{n+1/2}$ is the average value of c at the interface between Cells k–1 and k between time levels n and n+1. The salient point of the algorithm lies in the definition of the interface values $c_{k-1/2}^{n+1/2}$. In order to minimize numerical diffusion, we used an arbitrary time step explicit method presented in Leonard (1994). This method removes the restriction on the time computational time step by allowing the dimensionless CFL number $u\Delta t/\Delta x$ to take any arbitrary large value. Δt is set up to the largest possible value allowing the fastest region to travel over the length L of the computational domain within Δt, that is

$$\Delta t_{\max} = \frac{L}{\max_i u_i} \tag{A.4}$$

Equation (A.2b) is discretized using a classical centred implicit scheme

$$F c_{k-1}^{n+1} + (1 - 2F) c_k^{n+1} + F c_{k+1}^{n+1} = c_k^n \tag{A.5a}$$

$$F = \frac{D\Delta t}{\Delta x^2} \tag{A.5b}$$

Eq. (A.2c) is discretized using an implicit time marching scheme

$$\frac{\mathbf{c}_k^{n+1} - \mathbf{c}_k^n}{\Delta t} = \mathbf{R}\mathbf{c}_k^{n+1} \tag{A.6}$$

where $\mathbf{c} = [c_i]$. Solving (A.6) for $\mathbf{c}_k^{n+1}$ yields

$$\mathbf{c}_k^{n+1} = (\mathbf{I} - \Delta t \mathbf{R})^{-1} \mathbf{c}_k^n \tag{A.7}$$

Acknowledgements

The authors thank Jean-Philippe Chazarin from the laboratory HydroSciences Montpellier – France for his help in developing the electronic devices used in the experiments.

References

Bajracharya, K., and Barry, D. A., 1997. Nonequilibrium solute transport parameters and their physical significance: Numerical and experimental results. J. Contam. Hydrol., 24, 185-204.

Berkowitz, B., Cortis, A., Dror, I., Scher, H., 2009. Laboratory experiments on dispersive transport across interfaces: The role of flow direction. Water Resources Research, 45, W02201.

Berkowitz, B., Emmanuel, S., Scher, H. 2008. Non-Fickian transport and multiple-rate mass transfer in porous media. Water Resources Research, 44, W03402.

Bijeljic, B., and Blunt, M. J. (2006), Pore-scale modelling and continuous time random walk analysis of dispersion in porous media, Water Resour. Res., 42, W01202.

Brusseau, M. L., Gerstl, Z., Augustijn, D., Rao, P. S. C., 1994. Simulating solute transport in an aggregated soil with the dual-porosity model: Measured and optimized parameter values. J. Hydrol., 163, 187-193.

Coats, K. H., and Smith, B. D., 1964. Dead-end pore volume and dispersion in porous media. Soc. Pet. Eng. J., 4, 73-84. url: http://www.ipt.ntnu.no/~curtis/courses/Resevoir-Simulation/Keith-Coats-Publications/spe00647-Coats-Dead-End-Pore-Volume-and-Dispersion-in-Porous-Media.pdf

de Smedt, F., and Wierenga, P. J., 1984. Solute transfer through columns of glass beads. Water Resour. Res., 20, 225-232.

De Smedt, F., Wauters, F., Sevilla, J., 1986. Study of tracer movement through unsaturated sand. J. Hydrol., 85, 169–181.

Dewaide, L., Collon, P., Poulain, A., Rochez, G., Hallet, V., 2018. Double-peaked breakthrough curves as a consequence of solute transport through underground lakes: a case study of the Furfooz karst system Belgium. Hydrogeol. J., 26 (2), 641–650.

Farmer, C.L., 2022. Upscaling: a review. Intrnational Journal for Numerical Methods in Fluids, 40, 63–78.

Field, M.S., Leij, F.J., 2012. Solute transport in solution conduits exhibiting multi-peaked breakthrough curves. J. Hydrol., 440, 26–35.

Gaudet, J. P., Jégat, H., Vachaud, G., Wierenga, P. J., 1977. Solute transfer with exchange between mobile and stagnant water through unsaturated sand. Soil Sci. Soc. Am. J., 41, 665-671.

Goldscheider, N., Meiman, J., Pronk, M., Smart, C., 2008. Tracer tests in karst hydrogeology and speleology. Int. J. Speleol., 37 (1), 27–40.

Golfier, F., Quintard, M., Wood, B.D., 2011. Comparison of theory and experiment for solute transport in weakly heterogeneous bimodal porous media. Adv. Water Resour. 34, 899–914.

Griffioen, J. W., Barry, D. A., Parlange, J.-Y., 1998. Interpretation of two-region model parameters. Water Resources Research, 34 (3), 373-384.

Haggerty, R., Gorelick, S. M. 1995. Multiple-rate mass transfer for modelling diffusion and surface reactions in media with pore-scale heterogeneity. Water Resources Research, 31 (10), 2383-2400.

639 Haggerty, R., McKenna, S. A., and Meigs, L. C., 2000. On the late-time behaviour of tracer
640 test breakthrough curves, Water Resources Research, 36.12, 3467–3479.
641 Haggerty, R. Harvey, C. F., Freiherr von Schwerin, C., Meigs, L. C., 2004. What controls the
642 apparent timescale of solute mass transfer in aquifers and soils? A comparison of
643 experimental results. Water Resources Research, 40, W01510.
644 Hansen, S. K. 2022. Experimental support for a simplified approach to CTRW transport
645 models and exploration of parameter interpretation. Water Resources Research, 58,
646 e2021WR031350.
647 Jørgensen, P.R., Helstrup, T., Urup, J., Seifert, D., 2004. Modeling of non-reactive solute
648 transport in fractured clayey till during variable flow rate and time. Journal of
649 Contaminant Hydrology, 68, p. 193-216.
650 Khan, A. U.-H., and Jury, W. A., 1990. A laboratory study of the dispersion scale effect in
651 column outflow experiments. J. Contam. Hydrol., 5, 119-131.
652 Klafter, J., Blumen, A., Shlesinger M.F. 1987. Stochastic pathway to anomalous diffusion.
653 Physical Review A, 35, 3081-3085.
654 Koch, S ., and Flühler, H ., 1993. Non-reactive solute transport with micropore diffusion in
655 aggregated porous media determined by a flow interruption method. J. Contam. Hydrol.,
656 14, 39-54.
657 Kookana, R. S., Schuller, R. D., Aylmore, L. A. G., 1993. Simulation of simazine transport
658 through soil columns using time-dependent sorption data measured under flow
659 conditions. J. Contam. Hydrol., 14, 93–115.
660 Krupp, H. K., and Elrick, D. E., 1968. Miscible displacement in an unsaturated glass bead
661 medium. Water Resour. Res., 4, 809-815.
662 Le Borgne, T., D. Bolster, M. Dentz, P. de Anna, and A. Tartakovsky (2011), Effective pore-
663 scale dispersion upscaling with a correlated continuous time random walk approach,
664 Water Resour. Res., 47, W12538.
665 Leonard, B. P. 1994. Note on the von Neumann stability of explicit one-dimensional
666 advection schemes. Computer methods in applied mechanics and engineering, 118(1-2),
667 29–46.
668 Li, L., Barry, D. A., Culligan-Hensley, P. J., Bajracharya, K., 1994. Mass transfer in soils with
669 local stratification of hydraulic conductivity. Water Resources Research, 30, 2891-2900.
670 Majdalani, S., Chazarin, J. P., Delenne, C., Guinot, V., 2015. Solute transport in periodical
671 heterogeneous porous media: Importance of observation scale and experimental
672 sampling. Journal of Hydrology, 520, 52–60, doi.org/10.1016/j.jhydrol.2014.10.065
673 Majdalani, S., Guinot, V., Delenne, C., Gebran, H., 2018. Modelling solute dispersion in
674 periodic heterogeneous porous media: Model benchmarking against intermediate scale
675 experiments. Journal of Hydrology, 561, p. 427–443.
676 Maloszewski, P., Harum, T., Benischke, R., 1992. Mathematical modelling of tracer
677 experiments in the karst of Lurbach system. Steierische Beiträge zur Hydrogeologie, 43,
678 116–136.
679 Maraqa, M. A., 2001. Prediction of mass-transfer coefficient for solute transport in porous
680 media. Journal of Contaminant Hydrology, 50, 1–19.
681 Metzler, R., Klafter, J. 2000. The random walk's guide to anomalous diffusion: a fractional
682 dynamics approach. Physics Reports, 339, 1-77.
683 Moradi, G., and Mehdinejadiani, B., 2018. Modeling solute transport in homogeneous and
684 heterogeneous porous media using spatial fractional advection-dispersion equation. Soil
685 Water Research, 13: 18-28. doi: 10.17221/245/2016-SWR.
686 Nielsen, D. R., and Biggar, J. W., 1961. Miscible displacement in soils, Experimental
687 information. Soil Sci. Soc. Am. Proc., 25, 1-5.

Nkedi-Kizza, P., Biggar, J. W., Selim, H. M., van Genuchten, M. T., Wierenga, P. J., Davidson, J. M., Nielsen, D. R., 1984. On the equivalence of two conceptual models for describing ion exchange during transport through an aggregated oxisol. Water Resour. Res., 20, 1123-1130.

Perrin, J., Luetscher, M., 2008. Inference of the structure of karst conduits using quantitative tracer tests and geological information: example of the Swiss Jura. Hydrogeol. J., 16 (5), 951–967.

Rambow,J ., and B. Lennartz, 1993. Laboratory method for studying pesticide dissipation in the vadose zone. Soil Sci. Soc. Am. J., 57, 1476-1479.

Rao, P. S. C., Rolston, D. E., Jessup, R. E., Davidson, J. M., 1980. Solute transport in aggregated porous media: Theoretical and experimental evaluation. Soil Sci. Soc. Am. J., 44, 1139-1146.

Schulin, R., Wierenga, P. J., Fluhler, H., Leuenberger, J., 1987. Solute transport through a stony soil. Soil Sci. Soc. Am. J. 5, 36–42.

Selim, H. M., Schulin, R., Flühler, H., 1987. Transport and ion exchange of calcium and magnesium in an aggregated soil. Soil Sci. Soc. Am. J., 51, 876-884.

Seyfried, M. S., and Rao, P. S. C., 1987. Solute transport in undisturbed columns of an aggregated tropical soil: Preferential flow effects. Soil Sci. Soc. Am. J., 51, 1434-1444.

Sharma, P.K., Agarwal, P., Mehdinejadiani, B., 2022. Study on non-Fickian behaviour for solute transport through porous media. ISH Journal of Hydraulic Engineering, 28(sup 1): 171-179. https://doi.org/10.1080/09715010.2020.1727783.

Silliman, S.E., Simpson, E.S., 1987. Laboratory evidence of the scale effect in dispersion of solutes in porous media. Water Resour. Res. 23 (8), 1667–1673.

Smettem, K. R. J., 1984. Soil-water residence time and solute uptake, 3, Mass transfer under simulated winter rainfall conditions in undisturbed soil cores. J. Hydrol., 67, 235-248.

Sun, H., Zhang, Y., Chen, W., Reeves, D.M. 2014. Use of a variable-index fractional-derivative model to capture transient dispersion in heterogeneous media. Journal of Contaminant Hydrology, 137, 47-58.

Sun, L., Niu, J., Hu, B.X., Wu, C., Dai, H. 2020. An efficient approximation of non-Fickian transport using a time-fractional transient storage model. Advances in Water Resources, 135, 103486.

Sutton, O.F., Kessel, E.D., Gharedaghloo, B., Price, J.S., 2022. Characterizing the hydraulic and transport properties of a constructed coarse tailings sand aquifer. Journal of Contaminant Hydrology, 249, 104047, DOI: 10.1016/j.jconhyd.2022.104047

Tran Ngoc, T. D., Ahmadi, A., Bertin, H., 2020. Non-Fickian dispersivity investigation from numerical simulations of tracer transport in a model double-porosity medium at different saturations. Journal of Contaminant Hydrology, 234, 103678. DOI: 10.1016/j.jconhyd.2020.103678

van Genuchten, M. T., and Wierenga, P. J., 1976. Mass Transfer Studies in Sorbing Porous Media I. Analytical Solutions, Soil Sci. Soc. Am. J., 40.4, 473–480. doi: 10.2136/sssaj1976.

van Genuchten, M. T., and Wierenga, P. J., 1977. Mass transfer studies in sorbing porous media: experimental evaluation with tritium ($^3H_20$), Soil Sci. Soc. Am. J., 41, 272-278.

van Genuchten, M. T., Wierenga, P. J., O'Conner, G. A., 1977. Mass transfer studies in sorbing porous media: experimental evaluation with 2,4,5-T. Soil Sci. Soc. Am. J., 41, 278-285.

Yin, M. , Ma, R., Zhang, Y., Chen, K., Guo, Z., Zheng, C. 2022. A dual heterogeneous domain model for upscaling anomalous transport with multi-peaks in heterogeneous aquifers. Water Resources Research, 58, e2021WR031128.

List of Tables

Table 1. Values and symbols of the flow rates tested in step experiments on columns X_i (i = 1 to 3) also called MHPM A, MHPM B, and MHPM C

Symbol	Flow rate (l/h)	Experiment duration (min)	Sampling Interval (s)
Q_2	0.25	180	10
Q_4	0.5	90	10
Q_{10}	1.25	40	5
Q_{20}	2.5	20	5
Q_{40}	5	10	1
Q_{100}	12.5	3	1
Q_{200}	25	2	1

Table 2. Calibration results with all flow rates. The average and standard deviations in each row are computed row from the three values obtained from MHPMs A-C.

Parameter	MHPM A	MHPM B	MHPM C	Average	Standard dev.
α_1 (cm)	2.36	2.33	1.72	2.14	0.36
α_2 (m)	0.373	0.269	0.262	0.301	0.062
μ_1 (-)	0.294	0.288	0.270	0.284	0.012
v_1 (-)	0.598	0.546	0.593	0.579	0.029
k_{12} (m^{-1})	0.578	0.295	0.948	0.607	0.327
J (-)	7.05×10^{-4}	10^{-3}	1.47×10^{-3}	1.06×10^{-3}	3.9×10^{-4}
$J^{1/2}$ (-)	2.66×10^{-2}	3.17×10^{-2}	3.84×10^{-2}	3.22×10^{-2}	5.9×10^{-3}
σ_{av}	1.56×10^{-2}	0.76×10^{-2}	0.56×10^{-2}	0.96×10^{-2}	5.3×10^{-3}

Table 3. Calibration results without Q_{200}. The average and standard deviations in each row are computed row from the three values obtained from MHPMs A-C.

Parameters	MHPM A	MHPM B	MHPM C	Average	Standard dev.
α_1 (cm)	1.55	1.15	1.48	1.39	0.21
α_2 (cm)	0.334	0.291	0.283	0.303	0.024
μ_1 (-)	0.271	0.228	0.264	0.254	0.023
v_1 (-)	0.592	0.506	0.591	0.563	0.049
k_{12} (m^{-1})	0.898	0.707	0.823	0.809	0.096
J (-)	5.78×10^{-4}	6.86×10^{-4}	8.19×10^{-4}	6.94×10^{-4}	1.21×10^{-4}
$J^{1/2}$ (-)	2.40×10^{-2}	2.62×10^{-2}	2.87×10^{-2}	2.63×10^{-2}	2.4×10^{-3}
σ_{av}	1.68%	0.72%	0.51%	0.97×10^{-2}	6.3×10^{-3}

Table 4. Goodness-of-fit indicators for experimental vs. modelled C/C_0.

Flow rate	MHPM A			MHPM B			MHPM C		
	r^2	$J^{1/2}$	MBE	r^2	$J^{1/2}$	MBE	r^2	$J^{1/2}$	MBE
Q_2	0.998	5.16×10^{-3}	1.63×10^{-3}	0.994	1.07×10^{-2}	1.13×10^{-3}	0.991	2.35×10^{-3}	7.74×10^{-4}
Q_4	0.998	4.33×10^{-3}	1.55×10^{-3}	0.999	8.44×10^{-3}	-2.17×10^{-4}	0.997	4.34×10^{-3}	-1.71×10^{-3}
Q_{10}	0.995	4.89×10^{-3}	3.51×10^{-3}	0.997	7.01×10^{-3}	8.39×10^{-3}	0.999	3.66×10^{-3}	9.61×10^{-4}
Q_{20}	0.999	4.03×10^{-3}	3.74×10^{-4}	0.998	1.23×10^{-2}	9.05×10^{-3}	0.997	2.53×10^{-3}	1.23×10^{-3}
Q_{40}	0.999	2.87×10^{-3}	3.04×10^{-4}	0.999	6.33×10^{-3}	4.83×10^{-3}	0.999	4.80×10^{-3}	2.11×10^{-3}
Q_{100}	0.999	1.25×10^{-2}	-1.61×10^{-3}	0.995	8.15×10^{-3}	7.13×10^{-4}	0.997	1.83×10^{-3}	6.18×10^{-5}
Q_{200}	0.995	5.04×10^{-3}	2.52×10^{-3}	0.999	1.59×10^{-2}	-1.05×10^{-3}	0.992	1.08×10^{-2}	5.17×10^{-3}

Table 5. Dimensionless numbers for similarity analysis. The Reynolds number is computed as $Re = \frac{QD}{Av} = \frac{QLD}{V_0 \nu}$ and the Peclet number in region *k* as $\mathrm{Pe}_k = L/\alpha$.

MHPM	Re (–)	Pe_1 (–)	Pe_2 (–)
A	1.32 – 132	9.7	44.9
B	1.32 – 132	13.0	51.5
C	1.32 – 132	10.1	53.0

Figures

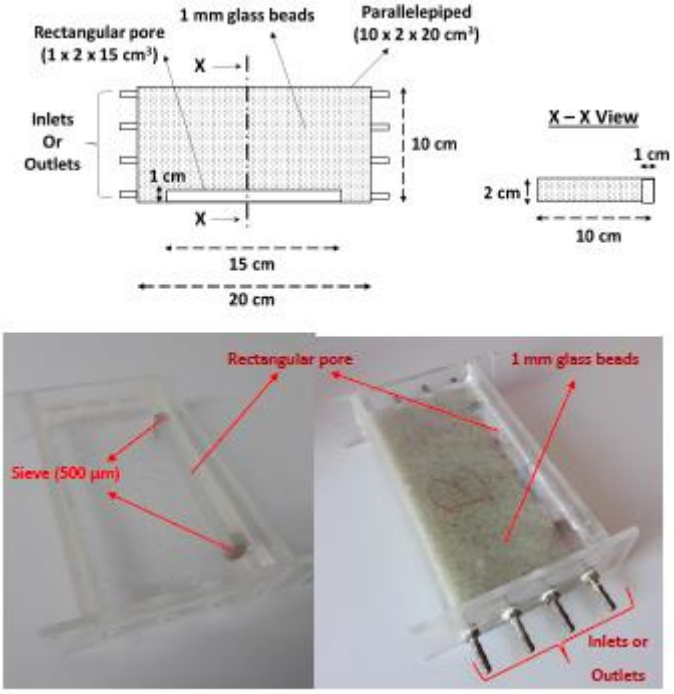

Figure 1. Model heterogeneous porous medium X_i (i = 1 to 3). Dashed area represents 1 mm glass beads and white area represents the heterogeneity (rectangular pore). Real photos show the column before and after filling it with 1 mm glass beads.

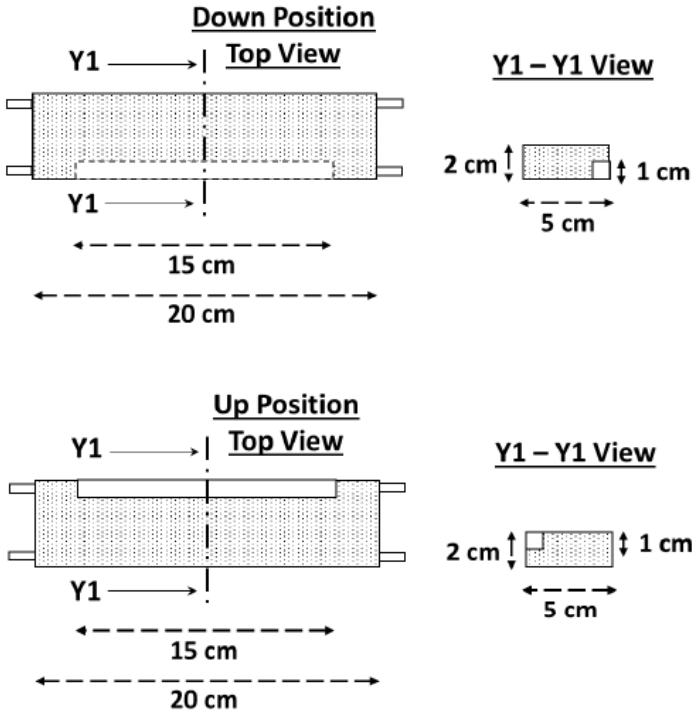

Figure 2. Model heterogeneous porous medium Y_1 where the heterogeneity (white rectangle) is located in one corner. As in Figure 1, dashed area represents 1 mm glass beads and white area represents the heterogeneity (rectangular pore).

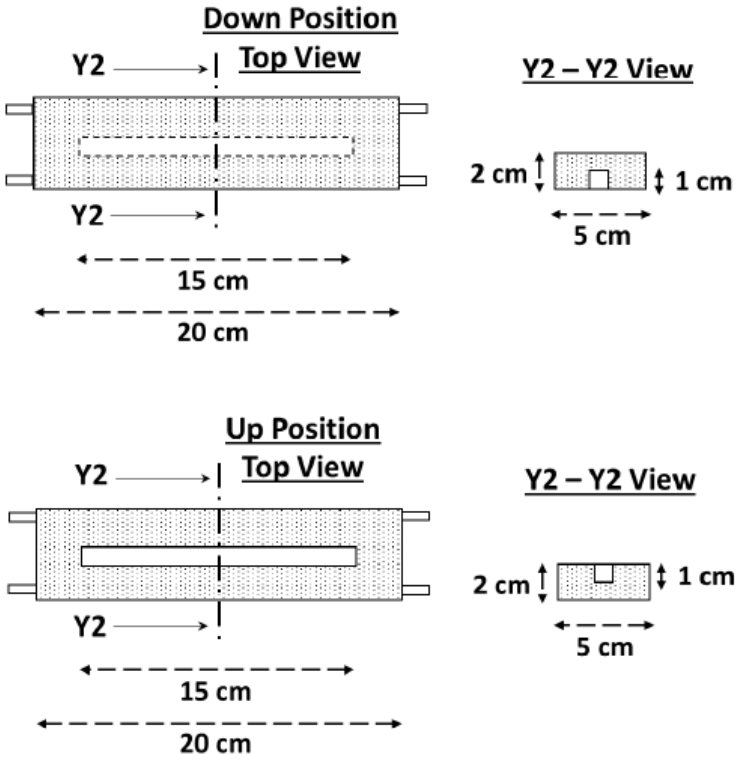

Figure 3. Model heterogeneous porous medium Y_2 where the heterogeneity (white rectangle) is located in the center of one face. As in Figure 1, dashed area represents 1 mm glass beads and white area represents the heterogeneity (rectangular pore).

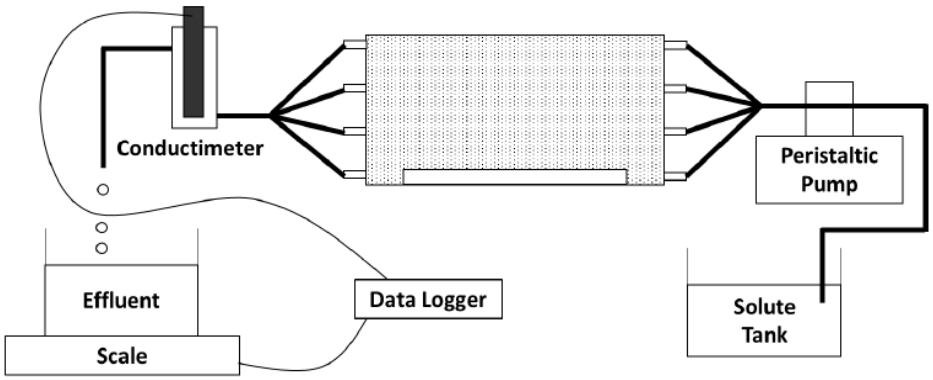

Figure 4. Tracer step experiment setup.

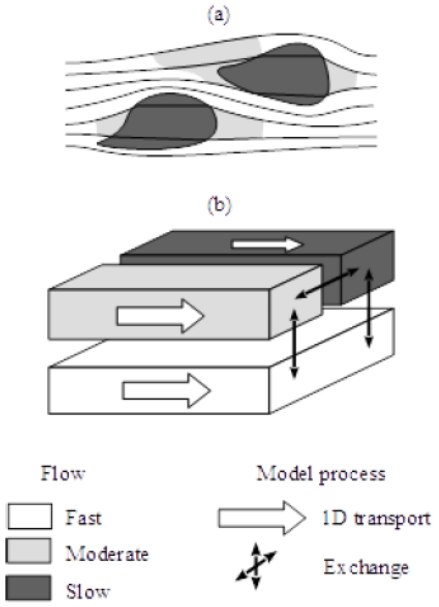

Figure 5. MRAD model definition sketch. (a) Streamlines and partition into several regions in the presence of heterogeneities. (b) Schematization in the MRAD model. Any of the fast, moderate or slow velocity regions may be partitioned into several subregions when required by the flow physics

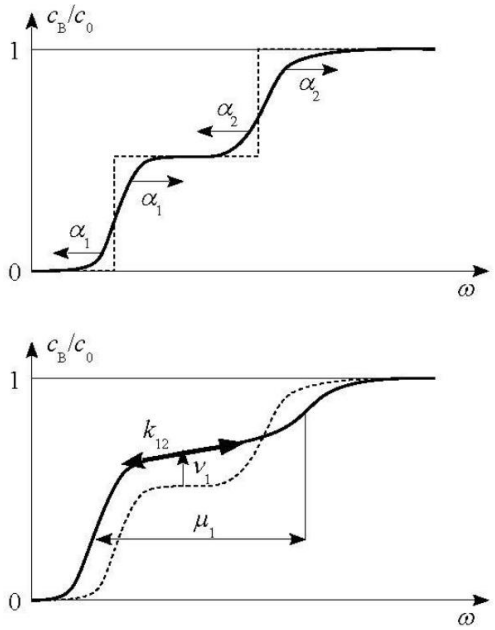

Figure 6. Influence of the MRAD parameters on the shape of the breakthrough curve.

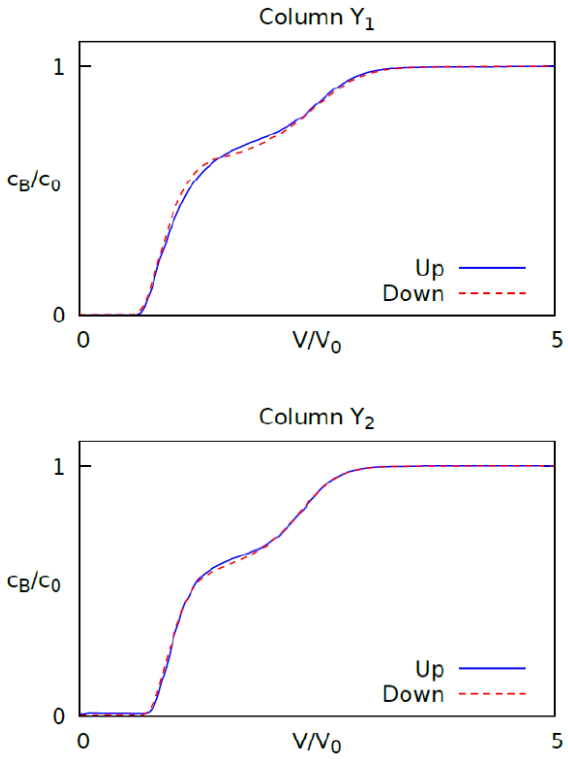

Figure 7. Step experiments with flow rate Q_{100}. Top: Column Y_1 in Up and Down positions. Bottom: Column Y_2 in Up and Down positions.

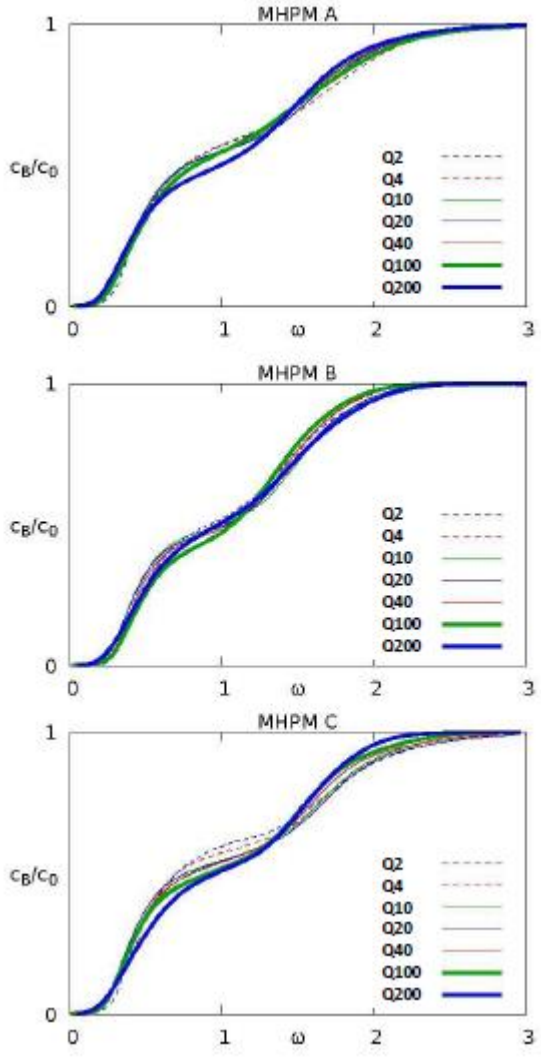

Figure 8. Experimental breakthrough curves for columns MHPM A, B, and C. The variable change $\omega = Qt/V_0$ is adopted for the abscissa axis. The three digit figures in the legend refer to the peristaltic pump setting, see Table 1 for the flow rate values.

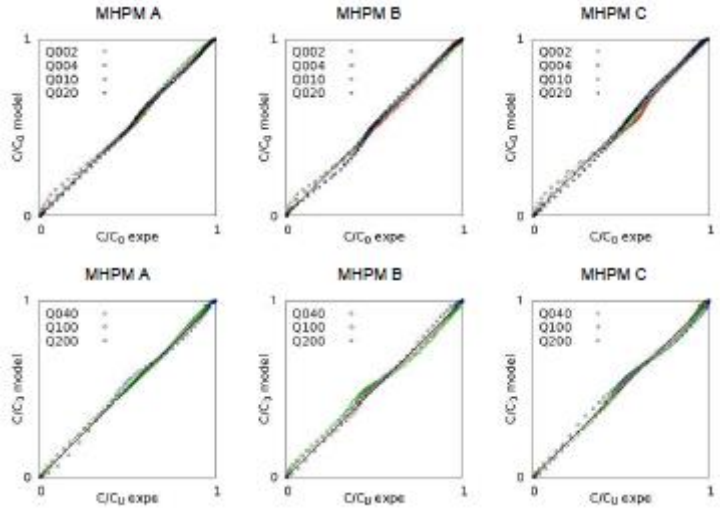

Figure 9. Experimental vs. modelled breakthrough curves for the three MHPM (A, B, and C) and for the seven tested flow rates.

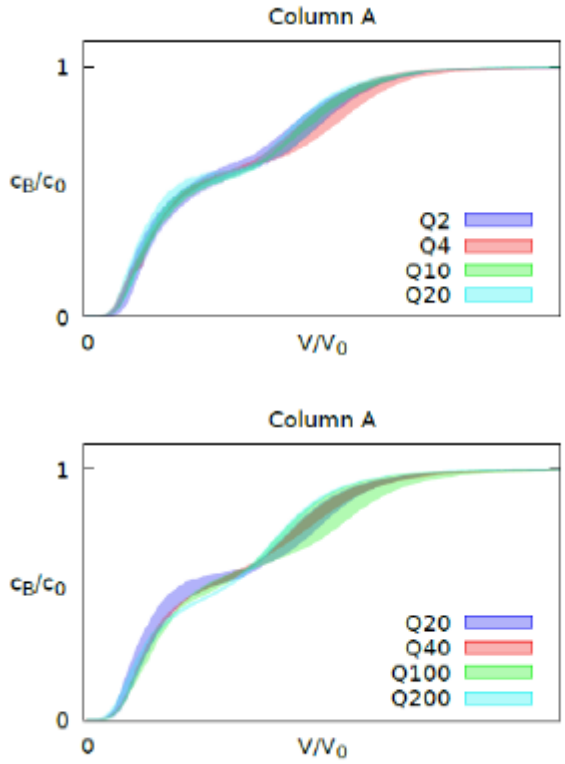

Figure S1. Experimental BTCs for MHPM A plotted along with their experimental uncertainty. Two plots are shown, with Q20 is common to both graphs for the sake of comparison.

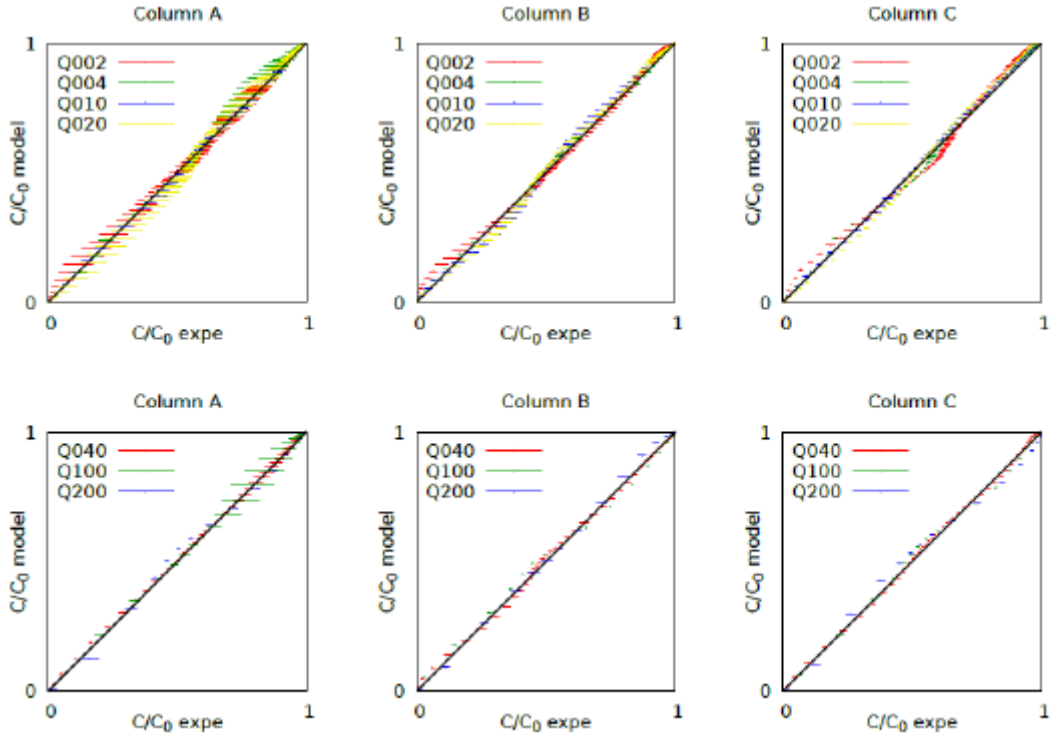

Figure S2. A modified version of Figure 9 that includes the experimental imprecision.